1
Impinging Jet Drying

Eckehard Specht

1.1
Application

Flat products such as tiles, tissue, paper, textiles and wood veneer are often dried using nozzle arrays (Mujumdar, 2007). Figure 1.1 illustrates the basic principle of the drying process using a nozzle array. Ambient air of temperature T_a is heated in a combustion chamber or in a heat exchanger to temperature T_0, requiring the energy $\dot{H}_0$. The heated air is blown through the nozzle array in order to dry the product. These conditions result in the product temperature T_S. The evaporating mass flow has the enthalpy $\dot{H}_\nu$. The nozzle array is characterized by the inner diameter d of the individual nozzle, by the pitch t between the nozzles, and the velocity w of the released gas.

There are basically three possible designs of nozzle arrays which differ with regard to the spent flow of the air (Fig. 1.2). In a field of individual nozzles the air can flow unimpeded between almost all nozzles; however, in a hole channel the air can flow only between those above. In a perforated plate the air can only continue to flow laterally and then escape. Hole channels and perforated plates are easier to produce than single nozzles, as they only require holes to be perforated. However, the heat transfer is the highest for nozzle fields and the lowest for perforated plates, as will be subsequently shown.

For the design of the nozzle array the energy consumption needed for drying is essential. This is the energy for heating the air:

$$\dot{H}_0 = \rho_0 \dot{V}_0 c_p (T_0 - T_a), \tag{1.1}$$

where T_0 and T_a represent the temperatures of the heated air and the environment, respectively, and c_P is the average specific heat capacity between these two temperatures. The density and the volume flow rate refer to the heated air. Volume flow rate depends on the discharge velocity w and the number n of the nozzles with a diameter of d:

$$\dot{V}_0 = n \frac{\pi}{4} d^2 w. \tag{1.2}$$

Modern Drying Technology Volume 5: Process Intensification, First Edition.
Edited by Evangelos Tsotsas and Arun S. Mujumdar.

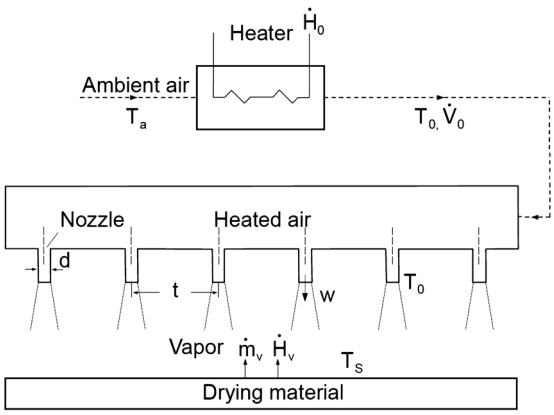

Fig. 1.1 Drying using a nozzle array.

The number of nozzles will depend on the nozzle pitch t and the surface area A of the material:

$$n = \frac{A}{t^2}. \tag{1.3}$$

The air temperature is calculated from the condition that the transferred heat has to cover the enthalpy of vaporization and the enthalpy to heat the dry material flow from ambient temperature to the saturation temperature T_S:

$$\alpha A(T_0 - T_S) = \dot{m}_v A \Delta h_v + \dot{M}_s c_s (T_S - T_a). \tag{1.4}$$

In Eq. 1.4, $\dot{m}_v$ is the evaporation flux, Δh_v is the evaporation enthalpy, and c_s is the specific heat capacity of the material. The evaporating mass flux is obtained from the relationship for the mass transfer

$$\dot{m}_v = \beta \frac{P}{R_v T_S} \ln \frac{P - P_a}{P - P_S}. \tag{1.5}$$

Here, the influence of one-side diffusion is taken into consideration. The gas constant of the vapor is represented by R_v, the total pressure by p, the partial pressure of the vapor in the ambient air by p_a, and the saturated vapor pressure by p_S. Additionally, the analogy of the Nusselt and Sherwood function is applied to the ratio of the heat and mass transfer coefficients:

$$\alpha = \beta \rho c_p Le^{0.6}, \tag{1.6}$$

wherein for the exponent of the Prandtl number in the Nusselt function the value 0.4 was used. The saturation pressure is approximated from the equilibrium relationship

$$P_S = P_0 \exp\left[-\frac{\Delta h_v}{R_v}\left(\frac{1}{T_S} - \frac{1}{T_0}\right)\right] \tag{1.7}$$

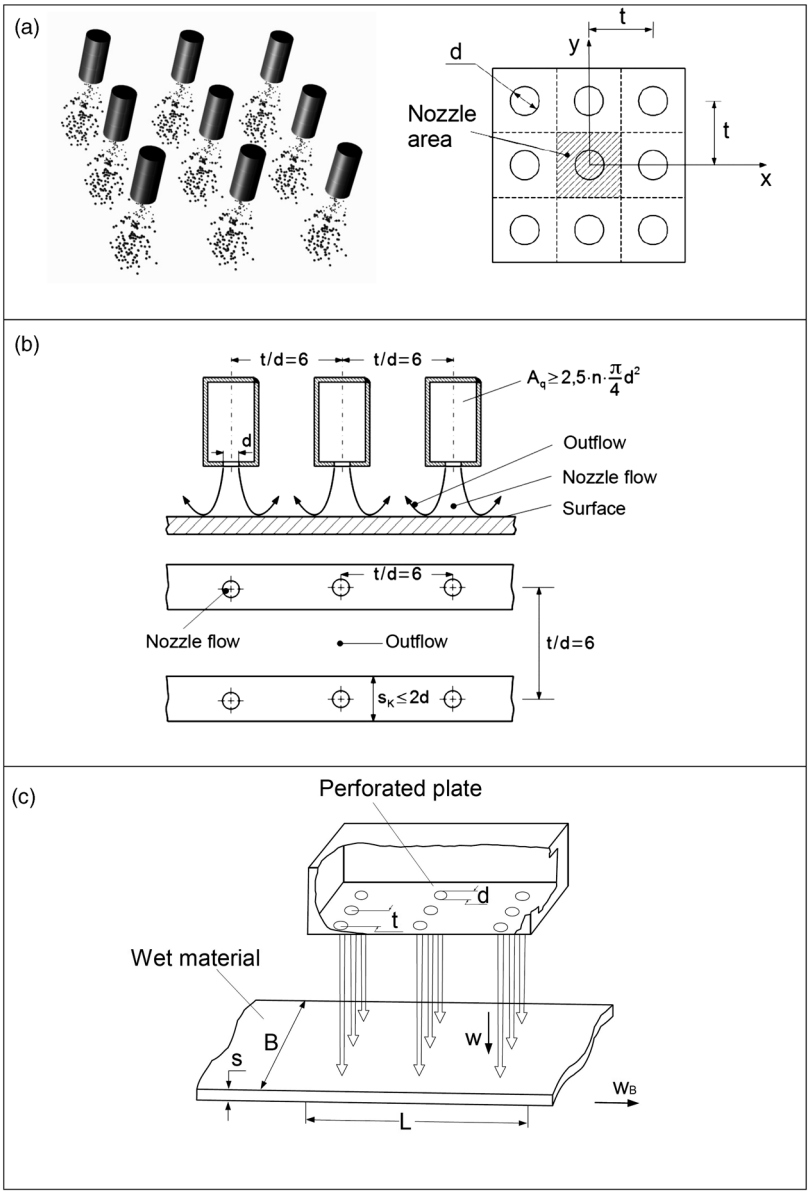

Fig. 1.2 Types of nozzle arrays. (a) Single-nozzle array; (b) Hole channel; (c) Perforated plate.

with the reference condition P_0, T_0, for example, $P_0 = 1$ bar, $T_0 = 373$ K. The minimum required energy is the enthalpy of vaporization of the water

$$\dot{H}_v = \dot{m}_v \, \Delta h_v. \tag{1.8}$$

The specific drying energy is the energy for heating the air $\dot{H}_0$ related to the enthalpy of evaporation. From the above equations results

$$\frac{\dot{H}_0}{\dot{H}_v} = \frac{\pi d^2 \rho_0 c_P w \left(\frac{\dot{m}_v \Delta h_v}{\alpha} + T_S - T_a \right)}{4t^2 \dot{m}_v \Delta h_v} = \frac{\pi d^2 \rho_0 c_P w}{4t^2} \left(\frac{1}{\alpha} + \frac{T_S - T_a}{\dot{m}_v \Delta h_v} \right). \quad (1.9)$$

The enthalpy to heat up the dry material was omitted for clarity purposes. Specific drying energy consumption according to Eq. 1.9 is dependent on the heat transfer coefficient. Particularly at high rates of evaporation, the specific energy consumption is lower with a high heat transfer coefficient. This strongly influences the drying rate and the size of the apparatus and, as a result, an increasing heat transfer coefficient increases the rate of drying which in turn allows a reduction in the size of the apparatus. The setting and the regulation of the heat transfer coefficient is therefore of great importance. The heat transfer of bodies in a crossflow is relatively low. In generating a high heat transfer, nozzle arrays are implemented wherein the jet emerging from the nozzles is perpendicular to the body. Such flows are called stagnation point flows. Nozzles may be either round or slot-shaped.

The fields of nozzles can be made from single nozzles, or hole channels, or from perforated plates with aligned or staggered arrangements, permitting a variety of geometric parameters. The heat transfer coefficient of nozzle arrays is therefore considered in more detail in the following.

1.2 Single Nozzle

First, an air jet emerging from a single nozzle is considered. In Fig. 1.3, the generated flow field of a nozzle is shown schematically. From the nozzle with the diameter d, the flow exits with the approximately constant speed w. The jet impinges the surface virtually unchanged with a constant velocity as long as

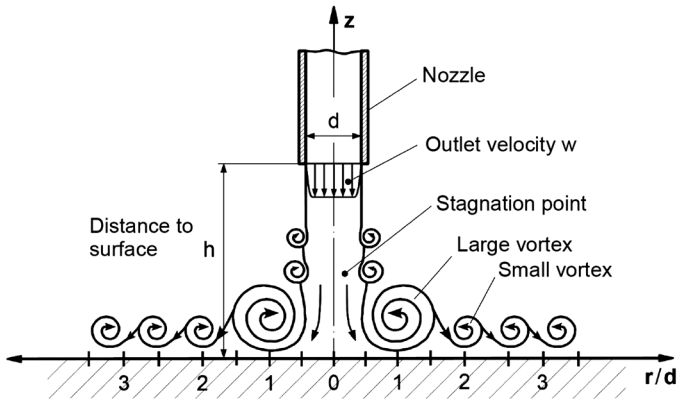

Fig. 1.3 Boundary layer of a stagnation point flow.

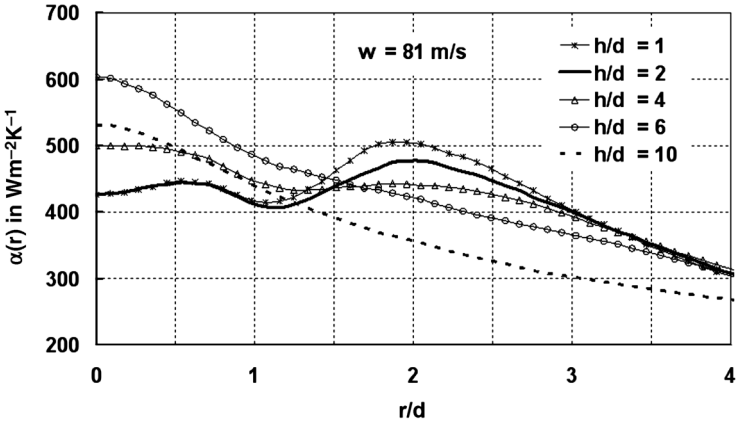

Fig. 1.4 Local heat transfer coefficients for a single nozzle.

the relative distance between the nozzle and the surface h/d is less than 6. At greater distances the core velocity decreases reducing the heat transfer. In the impinged zone, also called the stagnation point region, the flow is redirected in a radial direction, and in this region the flow can always be considered as laminar. At the outer edge of the emerging jet, circular vortices form. In the deflection region at $r/d \approx 1$, a large vortex forms but this disintegrates at approximately $r/d \approx 2$ into many small vortices. Eventually, the flow becomes increasingly turbulent (refer to Angioletti *et al.*, 2003, for photographs of the visualized flow). Increasing the nozzle distance from the stagnation point decreases the velocity, which in turn results in a decrease of the heat transfer coefficient. A completely laminar flow only occurs at Reynolds numbers smaller than 50; however, such small Reynolds numbers possess no meaning for technical heat-transfer processes.

The local heat transfer coefficient depends on three geometric dimensions: the nozzle diameter d; the nozzle distance h; and the radial distance r. Figure 1.4 shows the local heat transfer coefficients as a function of relative radius r/d with the relative distance h/d as a parameter exemplarily for a nozzle with a diameter of 10 mm and an outlet velocity of 81 m s^{-1}. It is evident for small distances of $h/d = 1$ to 4 that the heat transfer coefficient at the stagnation point ($r/d \leq 0.5$) is approximately constant, but then drops slightly to a relative minimum at $r/d \approx 1$. In the region of the vortex degradation at $r/d \approx 2$ the coefficient passes through a maximum and then decreases continuously. At radial distances $r/d > 3.5$, all profiles coincide for $h/d \leq 6$. Only higher distances result in a lower heat transfer.

For technical processes, the average heat transfer coefficient for a circular area,

$$\alpha = \frac{1}{\pi r^2} \int_0^r \alpha(r) 2\pi r dr, \tag{1.10}$$

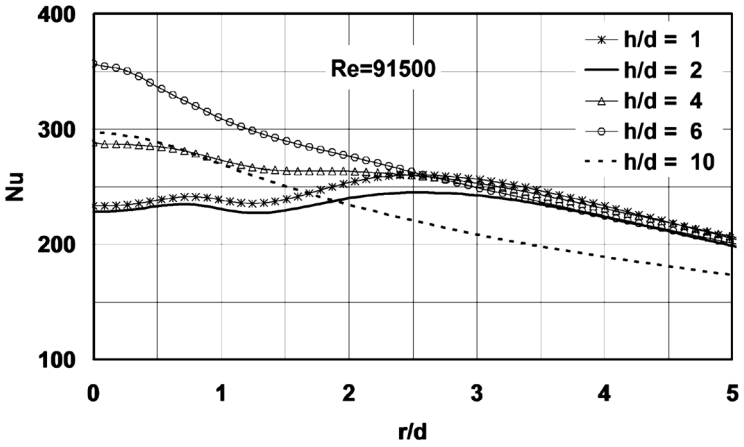

Fig. 1.5 Average Nusselt number of a single nozzle.

is of interest rather than the local heat transfer coefficient. The nozzle diameter exerts the greatest influence of all three geometric parameters. Therefore, the Nusselt number (Nu) and Reynolds number (Re) are defined as

$$\mathrm{Nu} = \frac{\alpha \mathrm{d}}{\lambda}, \mathrm{Re} = \frac{\mathrm{wd}}{\nu}. \tag{1.11}$$

In Fig. 1.5, the average Nusselt numbers are shown depending on the specific radius r/d, with the relative distance h/d as a parameter for a given Reynolds number. In the figure it is evident that from a distance of approximately $\mathrm{r/d} > 3$, all profiles coincide for $\mathrm{h/d} \leq 6$; greater distances will then result in a lower heat transfer.

As a consequence of Figs 1.4 and 1.5, it can be concluded that:

- The relative nozzle distance should be $\mathrm{h/d} < 6$ because for higher distances the heat transfer decreases. At a distance less than $\mathrm{h/d} = 4$, the local variation in the stagnation region increases.
- Up to relative stagnation point distances of approximately $\mathrm{r/d} = 3$, the average heat transfer is largely independent of the stagnation point distance. Only for greater distances will the heat transfer begin to decrease.

The Nusselt functions specified in the literature deviate from each other particularly with regard to the exponent of the Reynolds number; this is because the exponent depends on the radial distance. At the stagnation point the flow is always laminar, and the exponent is therefore 0.5. Turbulence fully develops only at a considerable distance from the stagnation point, and as a result the exponent must be 0.8. Figure 1.6 shows the increase of the exponent related to the radius (Adler, 2004). At a distance of $\mathrm{r/d} = 3$, the exponent has reached a value of only about 0.62. Different exponents are obtained depending on the size of the area considered in averaging.

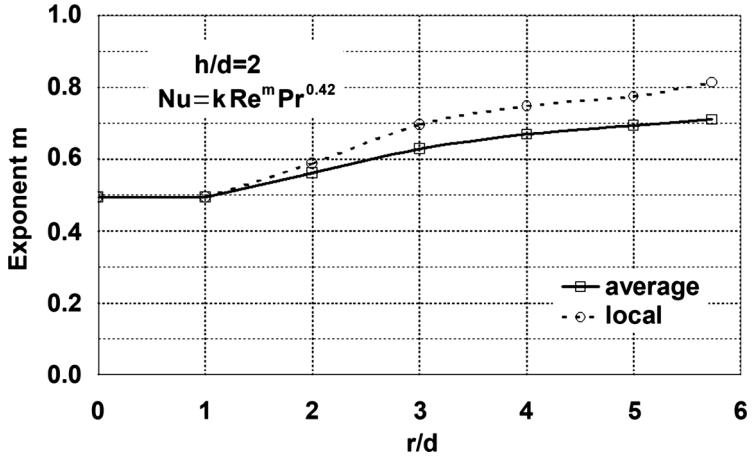

Fig. 1.6 Dependence of the exponent of the Reynolds number on distance.

The Nusselt functions reported in the literature for the stagnation point ($r/d \leq \pm 0.5$) can be approximated by

$$Nu_{St} = 0.72\ Re^{0.5}\ Pr^{0.4}. \tag{1.12}$$

For distances around $r/d = 3$, the average heat transfer can be accurately approximated with a power of 0.67

$$Nu = 0.12\ Re^{0.67}\ Pr^{0.4}. \tag{1.13}$$

In the literature, values ranging from 0.67 to 0.7 are mostly reported and, in order to improve comparability, in all of the following discussions the Reynolds exponent is approximated by 0.67. Nusselt functions are typically determined for air, which is the typical medium used during application.

1.3 Nozzle Fields

In the case of larger areas to be cooled or heated, several nozzles in a so-called nozzle field must be used. However, the relative nozzle pitch t/d must now be taken into consideration as an additional geometric parameter. Initially, arrays of single nozzles are discussed, and it is assumed that the pitch is equal in both directions.

1.3.1 Arrays of Single Nozzles

The profiles of the local Nusselt number Nu_{lo} for a row of three nozzles is shown in Fig. 1.7 (Attalla, 2005). Placement of the nozzles is indicated in the figure, where it can be seen how the typical profiles of the single nozzles overlap.

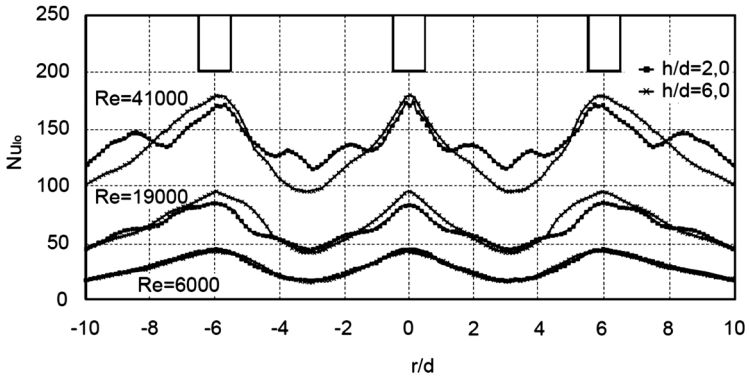

Fig. 1.7 Profiles of the local Nusselt number in an array of individual nozzles.

In Fig. 1.2a, the view of a nozzle array is shown with the impacted area. The nozzles may be arranged either in-line or staggered (in this figure the nozzles are in-line). In any case, each nozzle is influenced by the square area t^2 of the nozzle pitch, and by using this area the average of the heat transfer can be determined.

In Fig. 1.8, the average Nusselt number is shown in exemplary fashion as a function of the pitch t/d in an in-line assembly, with the relative nozzle distance h/d as a parameter for two Reynolds numbers. It is evident that a pitch of $t/d = 6$ will always result in a pronounced maximum.

In Fig. 1.9, the average Nusselt number is shown as a function of the relative nozzle distance with the pitch as a parameter. The profiles for both the in-line and staggered arrangements are shown. The Nusselt numbers are approximately constant up to a relative nozzle distance of about five, and then decrease continuously. When considering the profiles of the average Nusselt number, no significant difference can be seen between the in-line and staggered arrangements.

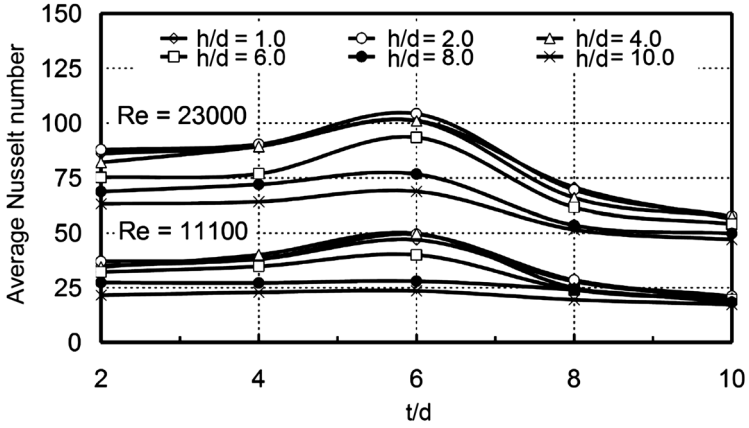

Fig. 1.8 Average heat transfer dependent on the pitch of the individual nozzles.

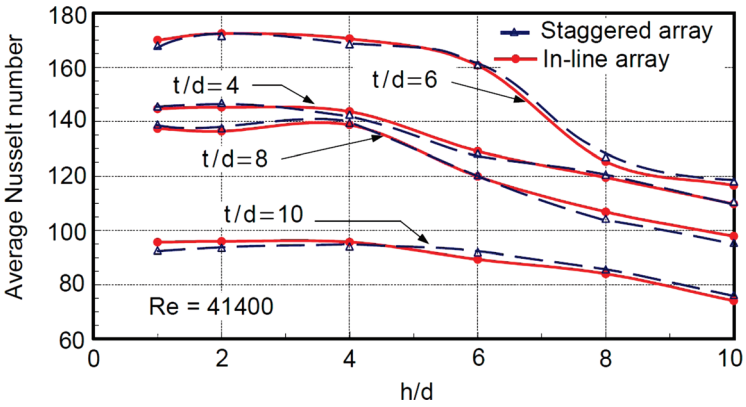

Fig. 1.9 Average heat transfer dependent on the relative nozzle distance.

However, the profiles of the local Nusselt number differ considerably (this point will be discussed further).

For $t/d = 6$ (maximum heat transfer), the Nusselt function in the stagnation area can be expressed as $r/d \leq \pm 0.5$

$$Nu_{St} = 0.82\ Re^{0.5}\ Pr^{0.4}; \tag{1.14}$$

The average Nusselt number over the entire surface area for $h/d < 5$ is

$$Nu = 0.16\ Re^{0.67}\ Pr^{0.4} \tag{1.15}$$

(Attalla and Specht, 2009).

In comparison with respect to the Nusselt functions for single nozzle (Eqs 1.12 and 1.13), it is evident that the heat transfer in the nozzle array is higher than that of the single nozzle under the condition of similar Reynolds numbers. Regarding the average heat transfer, this increase is approximately 30%.

In the following, the influence of the nozzle arrangement is considered in more detail. In Fig. 1.10 infrared images of the temperature field of a metal plate for both nozzle arrangements are shown. The average heat transfer is equal in both arrangements, as long as the relative nozzle distance is equal, as shown previously. However, there are differences in the profiles of the local heat transfer coefficient, and thus in the uniformity of heat transfer. In both images two lines are shown where the heat transfer is either maximal or minimal. The maximum heat transfer always occurs along the line passing through the stagnation points of the nozzles; accordingly, the minimum heat transfer always occurs on the line passing the middle between the stagnation points. As a consequence, the heat transfer is different in the longitudinal and transverse directions on a belt that passes beneath the nozzle array.

In Fig. 1.11 for a specific example, the profiles of the Nusselt number along the lines of the maximum and minimum heat transfer for the in-line arrangement and the staggered arrangement are shown, respectively. For the in-line arrangement,

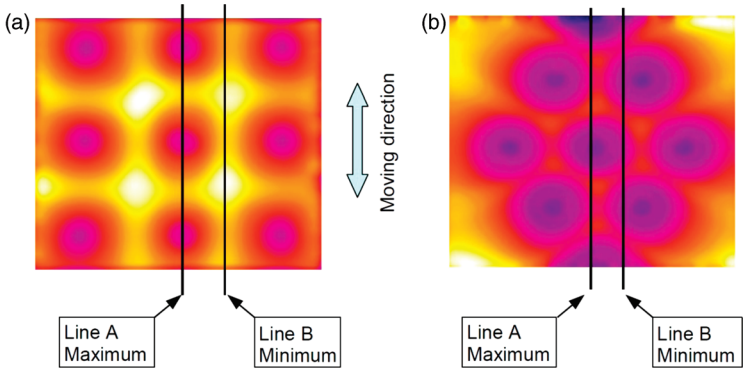

Fig. 1.10 Temperature field of a plate with (a) an in-line and (b) a staggered arrangement of the nozzles.

heat transfer along line A is always higher than along line B, so that the heat transfer is different in the cross-section. The high difference along line A is especially noteworthy. In this example the Nusselt number fluctuates between the values 19 and 3, which is approximately a factor of 6. Also on line B the Nusselt number fluctuates by about a factor of 4, and the heat transfer is therefore very uneven. In the staggered arrangement, both lines intersect so that the heat transfer takes alternatingly high and low values. It is also worth noting, that the differences

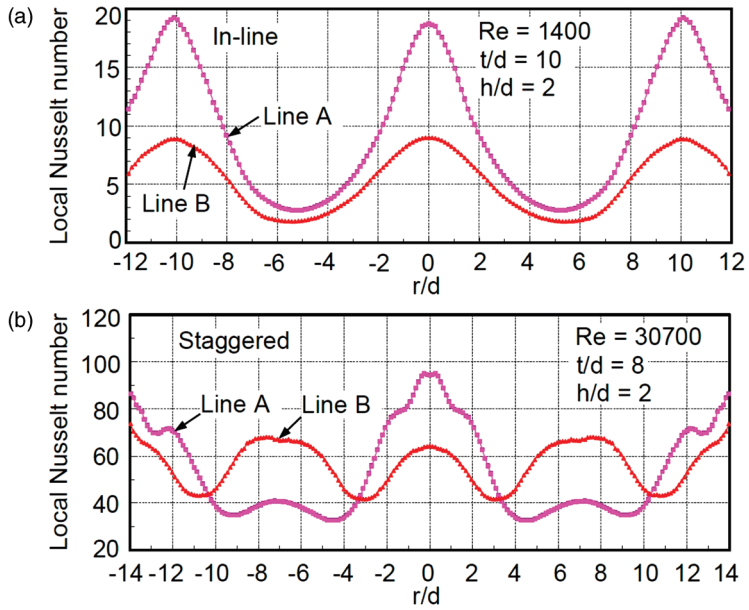

Fig. 1.11 Local heat transfer along lines A and B in (a) an in-line and (b) a staggered nozzle arrangement.

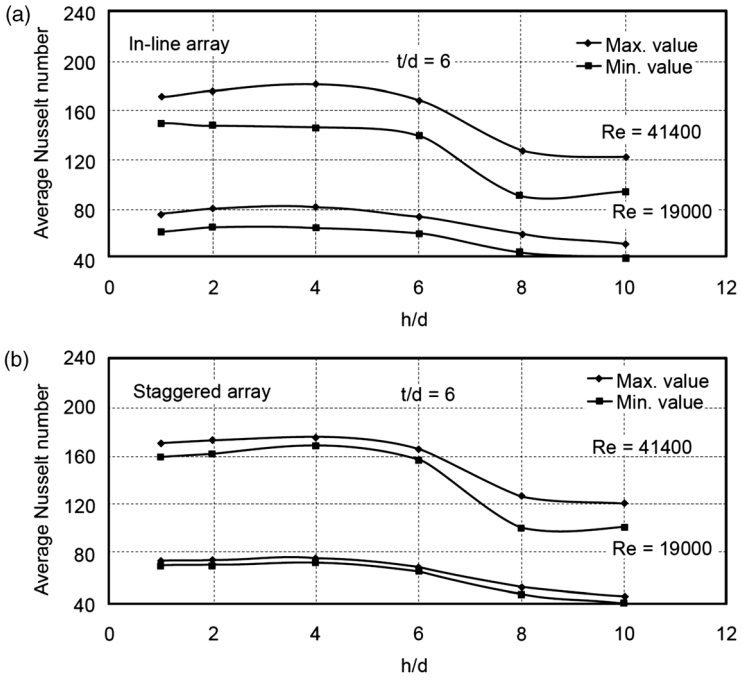

Fig. 1.12 Average heat transfer along lines A and B (cf. Fig. 1.10) in (a) an in-line and (b) a staggered arrangement.

between the maximum and minimum values of a line are significantly lower than for the in-line arrangement. On line A, the factor between the highest Nusselt number (95) and the lowest Nusselt number (32) amounted to only approximately three, compared to six for the in-line arrangement. Also, the difference between the maximum and minimum Nusselt numbers on line B for the staggered arrangement was less by a factor of 2 than for the in-line arrangement.

In Fig. 1.12, along lines A and B, the average Nusselt numbers for both arrangements are shown as a function of the relative distance for two Reynolds numbers at the optimum nozzle pitch. Up to a relative distance of 5, the Nusselt number is again approximately constant and then decreases. It is also significant that the average Nusselt number of line A (maximum value) for the in-line arrangement is always about 20% larger than that of line B (minimum value). In the staggered arrangement, however, no remarkable differences between the Nusselt numbers can be seen for the two lines. Therefore, although the difference between the two arrangements indicates that heat transfer for the staggered arrangement is much more uniform than for the in-line arrangement, the average heat transfer is approximately the same in both arrangements.

In Fig. 1.13, the average heat transfer coefficient for a nozzle array is shown as a function of the discharge velocity for selected nozzle diameters. It can be seen that

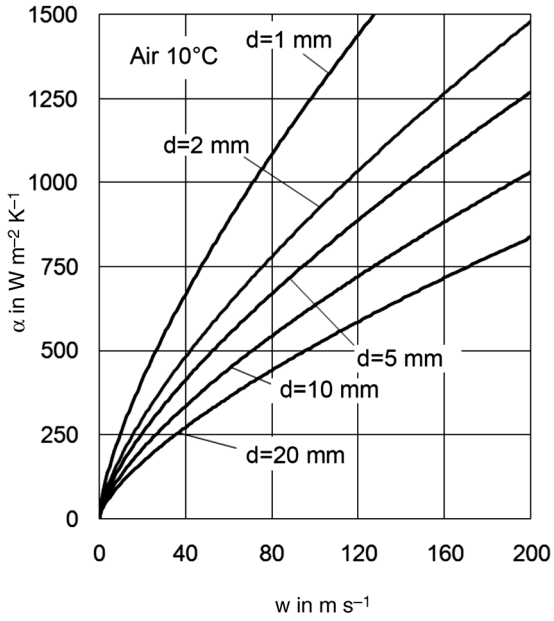

Fig. 1.13 Average heat transfer coefficient in a nozzle array.

it is possible for a nozzle array to achieve very high heat transfer coefficients in comparison to other forms of flow.

1.3.2 Hole Channels

Nozzle arrays are technically easier to manufacture in the form of hole channels than in the form of individual nozzles; such a hole channel is shown, in principle, in Fig. 1.2b.

In the rectangular channel, the holes are punched in the smaller lateral surface and serve as nozzle openings. In this case, the resistance of the outflow must be significantly higher than for the axial flow in the channel to ensure that the same amount of air emerges through all holes. This is usually the situation if the cross-sectional area of the channel is about 2.5-fold greater than the sum of the areas of the perforations. Uneven punching, for example by nonuniform ridges, will result in the jet streams not being perpendicular to the surface, and this in turn will lead to an uneven distribution of heat transfer.

In Fig. 1.14, the average heat transfer is shown as a function of the pitch of the perforations, for example for a Reynolds number with relative distance as a parameter. Regarding other Reynolds numbers in principle gives similar curves. Up to a pitch of about 6 the heat transfer will remain substantially constant, but after this point it will decrease. There is, therefore, no pronounced maximum at a

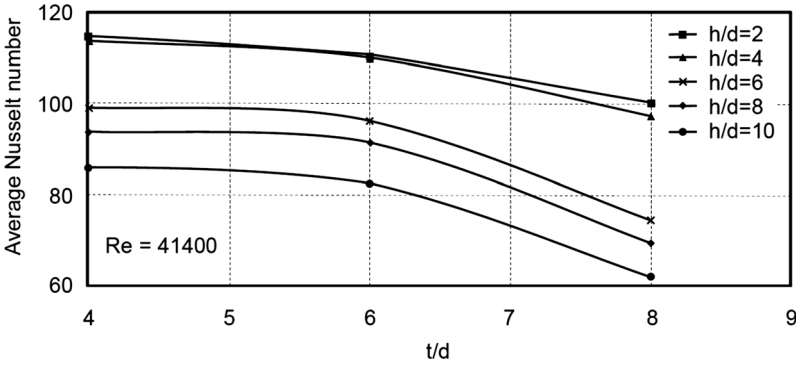

Fig. 1.14 Average heat transfer in a hole channel.

pitch of 6, as occurs with a field of individual nozzles, although at a smaller pitch the heat transfer will remain identical. Nonetheless it is recommended that, even with hole channels, a pitch is selected that is no less than 6 in order to minimize the flow rate, and thus the fan performance. The heat transfer will again be highest for relative nozzle distances in the range $2 < h/d < 5$, but will then decrease continuously with increasing distance.

The Nusselt functions for the stagnation point and the average value of the field can be approximated by (Attalla, 2005):

$$Nu_{St} = 0.47\,Re^{0.5}\,Pr^{0.4}, \tag{1.16}$$

$$Nu = 0.10\,Re^{0.67}\,Pr^{0.4}. \tag{1.17}$$

Based on comparisons with the corresponding functions for the single-nozzle array, it is evident that the heat transfer in hole channels is less, by about 35%.

1.3.3 Perforated Plates

In perforated plates, spent holes or slots must be installed so that the injected air can flow out again. The size and number of these outlets depends on the manufacturer of the perforated plates, and consequently various cross-flows can occur between the target area and the plate. How this affects the heat transfer is not yet known. Nonetheless, Martin (1977) developed a Nusselt function with which the heat transfer for a majority of perforated plates can be approximated, by providing the following correlation for aligned and hexagonally arranged perforations:

$$Nu = Re^{0.67}\,Pr^{0.42}\left[1 + \left(\frac{h}{d}\frac{F}{0.6}\right)^6\right]^{-0.05} F\frac{1 - 2.2\,F}{1 + 0.2(h/d - 6)F}. \tag{1.18}$$

Here, h/d is again the relative nozzle distance, and F is the square-root of the area ratio of the nozzle openings to the total area:

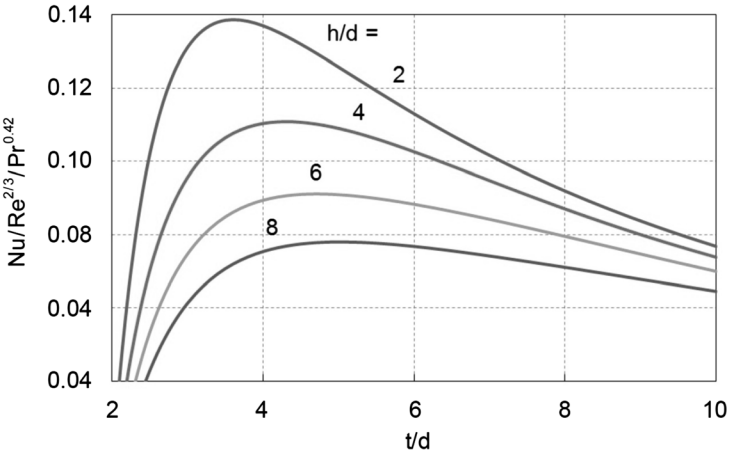

Fig. 1.15 Influence of the pitch and the nozzle distance on the heat transfer for perforated plates.

$$F = \sqrt{\frac{A_{nozzles}}{A_{total}}}. \tag{1.19}$$

For plates with equally distributed pitch t, it follows that

$$F = \sqrt{\frac{\pi}{4}}\frac{d}{t}. \tag{1.20}$$

The influence of the relative distance and the nozzle pitch is shown in Fig. 1.15, where heat transfer is seen to decrease continuously with the relative distance. The maximum heat transfer occurs in the case of pitches in the range of 3 to 5, depending on the distance. The heat transfer is lower than that of an array of individual nozzles. As the maximum occurs at a smaller pitch than 6 (as for single-nozzle arrays), a higher flow rate must also be applied.

Geers *et al.* (2008) have largely confirmed the correlation of Martin. Heikkilä and Milosavljevic (2002) concluded that the correlation provides slightly too-high values only when air temperature is above 400 °C. Huber and Viskanta (1994) provided a somewhat more simple correlation for pitches $t/d \geq 4$ right of the maximum (see Tab. 1.2), whereby the Nusselt number was seen to decrease continuously with the pitch.

1.3.4 Nozzles for Cylindrical Bodies

For nonplanar bodies the curvature arises as an additional geometric parameter. In the following discussions, a cylindrical body is considered as the fundamental case. In Fig. 1.16, a cylinder of diameter D is shown, which is impinged from a slot of

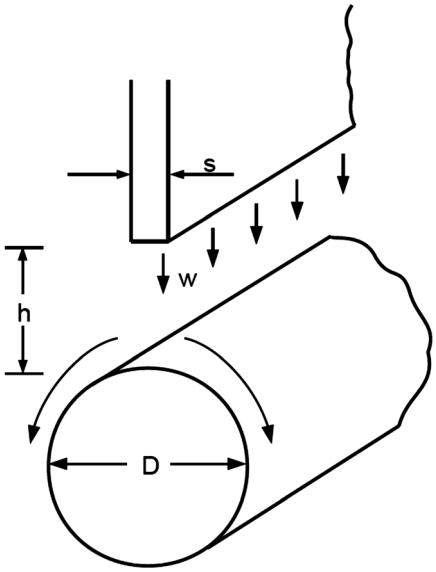

Fig. 1.16 Flow to a cylinder from a slot nozzle.

width s. With regards to the influence of the geometric parameters and the Reynolds number, divergent results have occasionally been reported in the literature. For example, Gori and Bossi (2003) and Chan *et al.* (2002) noted that a maximum in the heat and mass transfer occurred at a relative nozzle distance of $h/s = 8$, whereas Nada (2006) gave this maximum as between $h/d = 4$ and 6. McDaniel and Webb (2000) measured a maximum at $h/d = 5$, but only from nozzles with rounded edges. In contrast, for sharp-edged nozzles the heat transfer was continuously decreased with distance. Olsson *et al.* (2004) also indicated a decreasing heat transfer with distance, but this was very moderate with an exponent of only −0.077. For all of these authors the influence of the distance was weak. As noted previously for single nozzles and flat surfaces, a distance up to values of $h/d = 5$ had no effect, whereas heat transfer was slightly decreased at higher distances. The Nusselt functions given below are therefore based on a distance in the range $2 \leq h/s \leq 8$. The influence of the ratio D/s has been reported by the various authors with exponents ranging from 0.03 to 0.22; consequently, in order to provide a better comparison their results were approximated with an average exponent of 0.1.

The exponents for the Reynolds number specified by the above-mentioned authors have values from 0.4 to 0.82, depending partly on the geometric size. In Fig. 1.17, the measured Nusselt numbers of various authors are compared using $D/s = 2$ and $h/s = 5$ as examples. The length of the dotted lines represents the range of the investigated Reynolds numbers. The bold line with the gradient 0.67 represents an average value; this line can be approximated in

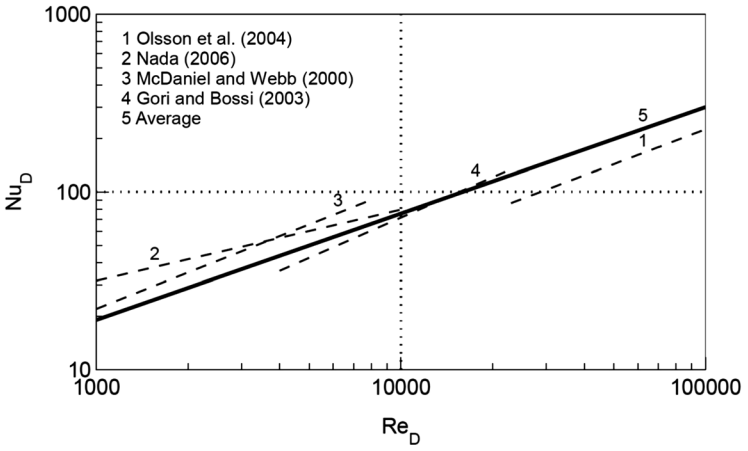

Fig. 1.17 Nusselt number dependent on the Reynolds number for cylinders with slot nozzles for $D/s = 2$ and $h/s = 5$.

the range $2 \leq h/s \leq 8$ with

$$Nu_D = 0.20\, Re_D^{0.67}\, Pr^{0.4} (D/s)^{0.1}. \tag{1.21}$$

The dimensionless numbers are formed with the cylinder diameter D:

$$Nu_D = \frac{\alpha\, D}{\lambda}, \quad Re_D = \frac{w\, D}{\nu}. \tag{1.22}$$

The values of the Nusselt numbers are similar to those resulting from the Nusselt function corresponding to cross-flow of cylinders if the cross-flow length $(\pi\, D)/2$ is used as a characteristic dimension in the Nusselt and Reynolds numbers.

The Nusselt function can alternatively be formed with the slot width s as the characteristic dimension resulting in

$$Nu_s = 0.15\, Re_s^{0.67}\, Pr^{0.4} (D/s)^{-0.23}, \tag{1.23}$$

with

$$Nu_s = \frac{\alpha s}{\lambda}, \quad Re_s = \frac{w s}{\nu}. \tag{1.24}$$

1.4 Summary of the Nusselt Functions

The Nusselt functions for the single nozzle are summarized in Tab. 1.1, and for the nozzle fields in Tab. 1.2. The Nusselt and Reynolds numbers are defined with the inner nozzle diameter d regarding round nozzles, and with the width s regarding slot nozzles. The exponent of the Reynolds number in correlations for the average

Tab. 1.1 Nusselt functions for single nozzles.

Nozzle shape	Nusselt function	Scope	Reference
Circular	Stagnation point region $Nu_d = 0.72\ Re_d^{0.5}\ Pr^{0.4}$	r/d $\leq \pm 0.5, 2 \leq h/d \leq 5$	Attalla and Specht (2009)
Slot	$Nu_s = 0.70\ Re_s^{0.5}\ Pr^{0.4}$	$2 \leq h/s \leq 5$	Vader *et al.* (1991)
Circular	Averaged values $Nu_d = 0.12\ Re_d^{0.67}\ Pr^{0.4}$	$0 < r/d < 3$	Adler (2004)

Tab. 1.2 Nusselt functions for nozzle fields impinging flat surfaces.

Arrays of individual nozzles (in-line or staggered):	
Stagnation point $r/d \leq 1$: $Nu_d = 0.82\ Re_d^{0.5}\ Pr^{0.4}$ Average: $Nu_d = 0.16\ Re_d^{0.67}\ Pr^{0.4}$ Pitch $t/d = 6$, Distance $2 \leq h/d \leq 5$	Attalla and Specht (2009)
Hole channels:	
Stagnation point $r/d \leq 1$: $Nu_d = 0.47\ Re_d^{0.5}\ Pr^{0.4}$ Average: $Nu_d = 0.10\ Re_d^{0.67}\ Pr^{0.4}$ Pitch $t/d \leq 6$, Distance $2 \leq h/d \leq 4$, Width $s_K/d \leq 2$	Attalla and Specht (2009)
Perforated plates: $Nu_d = Re_d^{0.67}\ Pr^{0.42}\left[1 + \left(\frac{h}{d}\frac{F}{0.6}\right)^6\right]^{-0.05} F\frac{1 - 2.2\,F}{1 + 0.2(h/d - 6)F}$ $F = \sqrt{\frac{A_{nozzles}}{A_{total}}}$, $F(\text{round nozzle}) = \sqrt{\frac{\pi}{4}}\frac{d}{t}$ Pitch $1.4 \leq t/d \leq 14$, Distance $2 \leq h/d \leq 12$	Martin (1977)
$Nu_d = 0.43\ Re_d^{0.67}\ Pr^{0.4}(h/d)^{-0.123}(t/d)^{-0.725}$ Pitch $4 \leq t/d \leq 8$, Distance $0.25 \leq h/d \leq 6$	Huber and Viskanta (1994)

heat transfer in nozzle fields has various reported values ranging from 0.66 to 0.72. It is mostly a matter of choice which exponent is used for the approximation of data within the spread of the measurement results. In order to enhance comparability of the Nusselt functions, the measurement results of the various references were respectively approximated by the exponent 0.67.

1.5 Design of Nozzle Field

Based on the given Nusselt functions for the required heat transfer coefficient in Eq. 1.9, nozzle arrays can now be designed. It is again assumed that the heat is predominantly transferred for evaporation, while the enthalpy to heat up the dry material is again neglected. First, an array of individual nozzles will be considered for which a distinct maximum in the heat transfer results at a pitch of $t = 6d$. Thus,

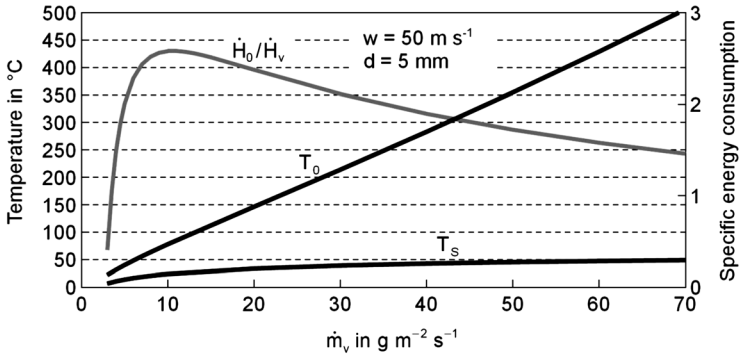

Fig. 1.18 Specific energy consumption, air, and product temperature as a function of the drying rate.

for the heat transfer coefficient from Eq. 1.15 with Pr = 0.7, is obtained:

$$\alpha = 0.14 \frac{\lambda}{\nu^{0.67}} w^{0.67} d^{-0.33}. \tag{1.25}$$

The material properties are to be formed with the average temperature $(T_0 + T_S)/2$. The specific energy consumption thus depends only on the three parameters – $\dot{m}_v$, d, and w – the influence of which must be calculated numerically.

In Fig. 1.18, the specific energy consumption, as well as the air and product temperatures, are shown as a function of the drying rate. As an example, a velocity of 50 m s^{-1}, a nozzle diameter of 5 mm, and an ambient temperature of 20 °C was used. The higher the drying rate, the more the air must be heated to achieve the enthalpy of evaporation because the velocity, and therefore the flow rate, remain constant. The air does not need to be heated for drying rates less than about 2 g m^{-2} s^{-1}, as an ambient air temperature of 20 °C is sufficient. Consequently, the specific energy consumption will be zero. At higher drying rates, the specific energy consumption is initially increased sharply and then passes through a maximum; however, the specific energy consumption decreases steadily thereafter.

In Fig. 1.19, specific energy consumption is shown separately as a function of the evaporation rate, with the nozzle diameter as a parameter. The nozzle exit velocity is assumed to be constant at 50 m s^{-1}. It is evident that the specific energy consumption is less with smaller nozzles, with the maximum being displaced towards higher evaporation rates. However, the lowest possible value of nozzle diameter is limited, first by the increase in production costs, and second through the minimum distance of the nozzle to the product. This distance should not be greater than approximately five-times the nozzle diameter; otherwise the heat transfer will be decreased. Rather, the smaller the nozzle the closer the field must be shifted towards the product.

In Fig. 1.20, specific energy consumption is shown as a function of the drying rate, with the nozzle discharge velocity as a parameter; as an example, a nozzle

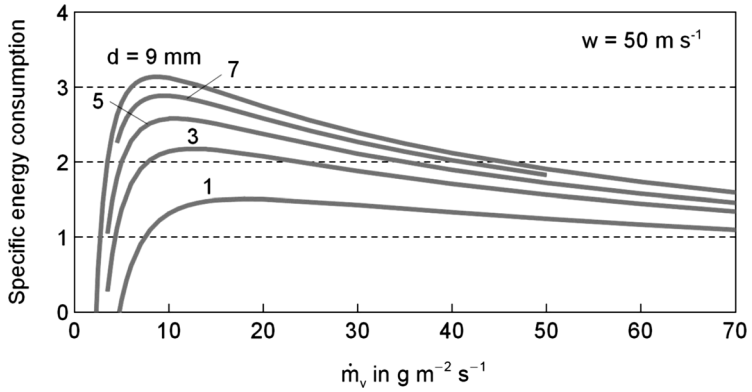

Fig. 1.19 Specific energy consumption as a function of the drying rate for different nozzle diameters.

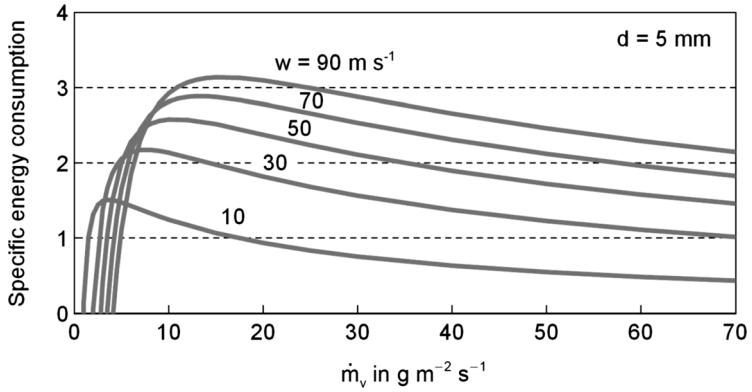

Fig. 1.20 Specific energy consumption as a function of the drying rate for different air velocities.

diameter of 5 mm is used. Here, the lower the discharge velocity, the lower is the specific energy consumption, and the maximum is shifted towards lower drying rates.

Lower velocities have the further advantage that only a small pressure drop, and therefore less fan power, will be required. However, the gas (i.e., the air) must be heated to higher temperatures in order to transfer the heat required. In Fig. 1.21, the heating temperature of the nozzle flow is shown as a function of the drying rate, with the nozzle exit velocity as a parameter; the nozzle diameter is again 5 mm. The required temperature increases approximately linearly with the drying rate, and the lower the velocity the steeper the gradient. The lowest value of the velocity is thus limited by the maximum temperature of the gas flow. This maximum temperature is dependent on the type of apparatus used for heating, the material strength, and the thermal sensitivity of the product. Due to the strength of the steel material the gas temperatures are generally limited to 500 °C.

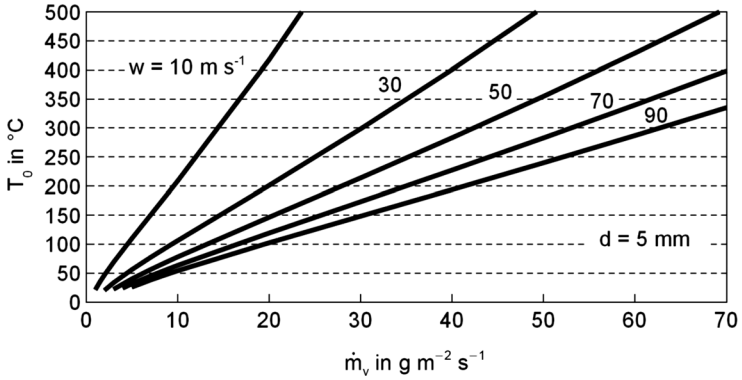

Fig. 1.21 Influence of the drying rate and the velocity on the required air temperature.

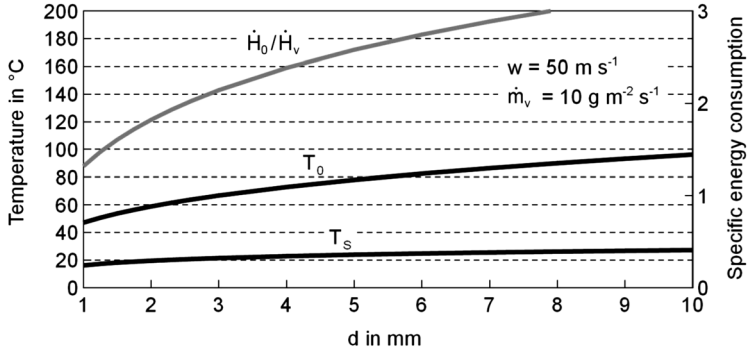

Fig. 1.22 Influence of the nozzle diameter.

Figures 1.22 and 1.23 show the specific energy consumption, the product temperature and the gas temperature as a function of the nozzle diameter and of the discharge velocity, respectively, as an example for the drying rate $10\,g\,m^{-2}\,s^{-1}$. All three parameters decrease with decreasing nozzle diameter, while the gradients become larger with smaller nozzle diameters. With decreasing velocity the specific energy consumption also decreases and both temperatures are increased. The lower the velocity, the larger is the gradient of variation of the considered parameters.

For hole channels, analogous results are valid, and a pitch of $t = 6d$ is again recommended. A larger pitch will result in a decrease in the heat transfer, which will remain constant with lower pitches; however, the number of nozzles and thus the flow rate, will be increased. The specific energy consumption and the required gas temperatures are slightly higher for hole channels than for single-nozzle arrays, because the heat transfer is somewhat lower.

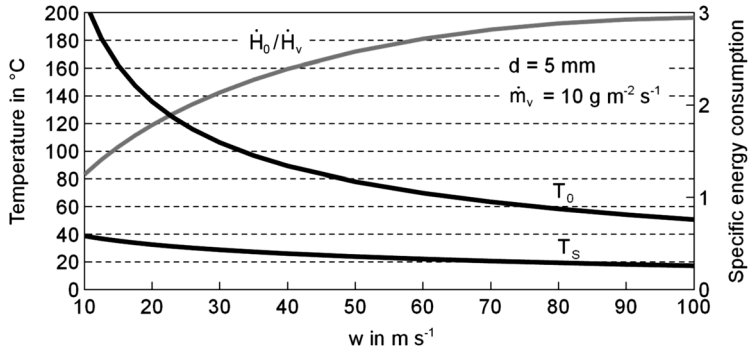

Fig. 1.23 Influence of the air velocity.

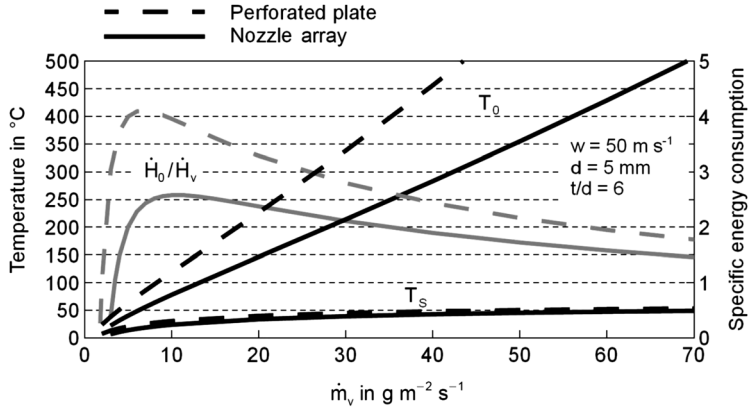

Fig. 1.24 Comparison of single-nozzle array and perforated plate for different drying rates.

In the case of perforated plates the heat transfer is somewhat less but they are the easiest to manufacture and consequently are commonly used. In Fig. 1.24, the specific energy consumption, the air temperature and the temperature of the material are again shown as a function of the drying rate, with a pitch of t = 6d as an example. The values for the perforated plate are compared here with values for the single-nozzle array. It is clear that, in order to achieve the same drying rate with perforated plates, higher air temperatures – and thus higher specific energy consumptions – are required to compensate for the reduced heat transfer.

Figure 1.25 shows the influence of the diameter on specific energy consumption and both temperatures, using examples of drying rates of $10\,g\,m^{-2}\,s^{-1}$ and of $50\,g\,m^{-2}\,s^{-1}$; the pitch is again t = 6d. When the drying rate is $10\,g\,m^{-2}\,s^{-1}$, the specific energy consumption of the perforated plate is almost 50% higher than that of the single-nozzle array. However, at a higher drying rate of $50\,g\,m^{-2}\,s^{-1}$ for diameters larger than 3 mm, the material can no

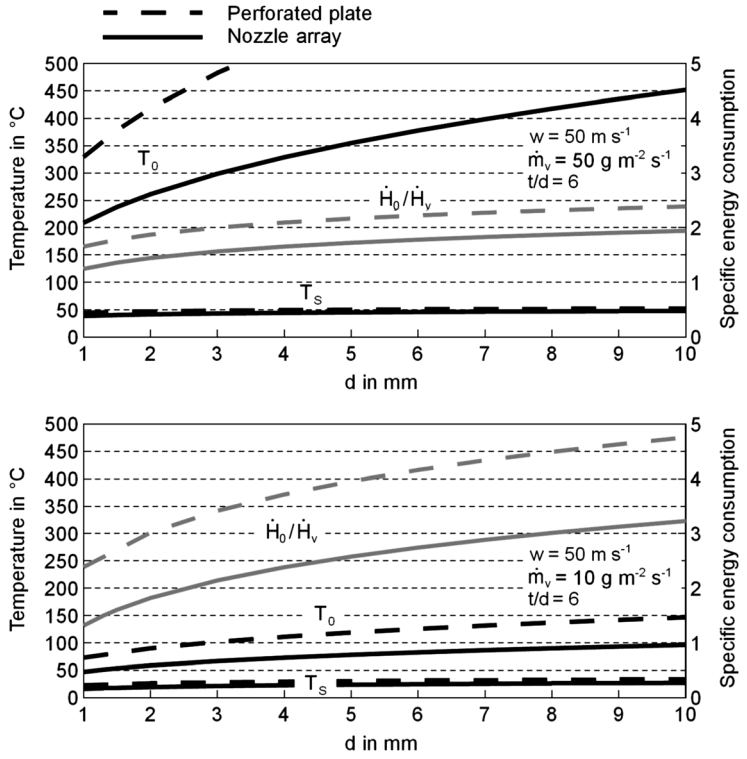

Fig. 1.25 Influence of the nozzle diameter for two drying rates.

longer be dried; otherwise, the air temperatures must be above 500 °C. With regards to perforated plates, the heat transfer according to Fig. 1.15 also depends on the pitch and nozzle distance. Thus, the maximum heat transfer will occur with a pitch in the range of four, which is a smaller value than for single-nozzle arrays. Heat transfer will also depend on the nozzle distance, and increases with decreasing distance. The influence of the pitch is shown for perforated plates in Fig. 1.26, where the pitch is with four smaller than before and with eight greater than before, while the diameter and velocity are held constant. With regards to the pitch of four, lower air temperatures will be needed as the heat transfer will be stronger, although the flow rate will be increased due to the larger number of perforations and, as a result, the specific energy consumption will also increase. In terms of low energy consumption, a large pitch is desirable; however, the maximum possible drying rates are limited due to increasing temperatures.

Finally, the influence of the nozzle distance is shown in Fig. 1.27 where, the lower the distance, the lower is the energy consumption. For a given air temperature with lower distances, higher drying rates can be achieved.

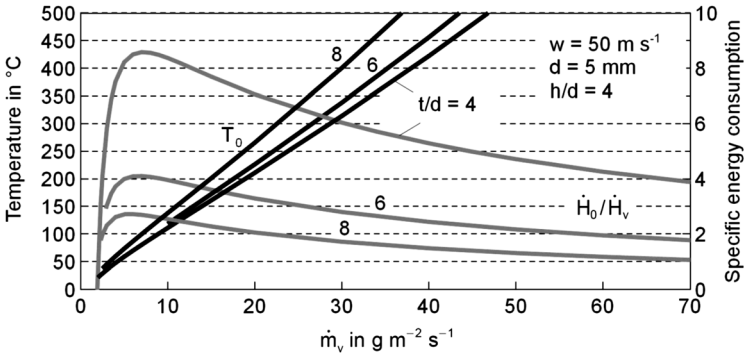

Fig. 1.26 Influence of the pitch for perforated plates at different drying rates.

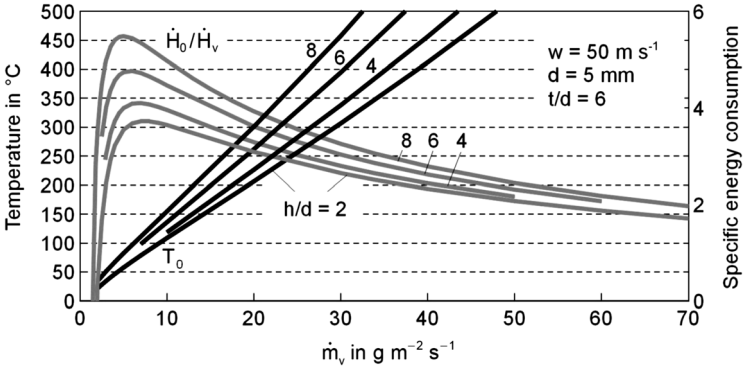

Fig. 1.27 Influence of the nozzle–surface distance for perforated plates.

1.6 Conclusion

The highest convective heat transfer coefficients in drying processes can be achieved using nozzle fields, and drying is strongly intensified in such a field. As a consequence, the heat transfer area, and therefore the size of the apparatus, can be reduced, saving investment costs.

The energy required to heat the drying air decreases with smaller nozzle diameters and slower outflow velocities, and consequently the operation costs are reduced. The lowest possible value of the nozzle diameter is, however, limited to ensure that the distance between the nozzle and material is not below four diameters. The lower the air velocity, the higher the hot air temperature must be. The temperature of the hot air is limited to 500 °C due to the strength of steel; however, the hot air temperature must normally be kept much lower in order to protect sensitive products against thermal damage. The pitch of the nozzles has an optimum value of six diameters for

the heat transfer with regards to single-nozzle arrays and hole channels. With regards to perforated plates, the optimum value for heat transfer occurs at pitches in the range of four, while the minimum for the specific energy consumption is achieved with a nozzle pitch of between eight and ten.

Additional Notation Used in Chapter 1

D	diameter of cylindrical drying body	m
d	inner diameter of nozzle	m
F	square-root of nozzle opening area to total area	–
$\dot{H}$	enthalpy flow rate	$J\ s^{-1}$
h	nozzle distance from product	m
m	exponent of Reynolds number	–
s	slot width, thickness	m
t	pitch between nozzles	m

Subscripts

lo	local value
s	saturation (assumed product condition)
st	stagnation point/region
0	outlet of heater (entrance of dryer)

References

Adler, W., 2004. Experimentelle Bestimmung des Wärmeübergangs bei der Prallströmung über einen hohen Reynoldszahlenbereich mittels Infrarot-Thermografie. Diss., Otto von Guericke University Magdeburg, Germany.

Angioletti, M., Di Tommaso, R. M., Nino, E., Ruocco, G., 2003. Simultaneous visualization of flow field and evaluation of local heat transfer by transitional impinging jets. *Int. J. Heat Mass Transfer* **46**: 1703–1713.

Attalla, M., 2005. Experimental investigation of heat transfer characteristics from arrays of free impinging circular jets and hole channels. Diss., Otto von Guericke University Magdeburg, Germany.

Attalla, M., Specht, E., 2009. Heat transfer characteristics from in-line arrays of free impinging jets. *Heat Mass Transfer* **45**(5): 537–543.

Chan, T. L., Leung, C. W., Jambunathan, K., Ashforth-Frost, S., Zhou, Y., Liu, J. H., 2002. Heat transfer characteristics of a slot jet impinging on a semi-circular convex surface. *Int. J. Heat Mass Transfer* **45**: 993–1006.

Geers, L. F. G., Tummers, M. J., Bueninck, T. J., Hanjalic, K., 2008. Heat transfer correlation for hexagonal and in-line arrays

of impinging jets. *Int. J. Heat Mass Transfer* **51**: 5389–5399.

Gori, F., Bossi, L., 2003. Optimal slot height in the jet cooling of a circular cylinder. *Appl. Therm. Eng.* **23**: 859–870.

Heikkilä, P., Milosavljevic, N., 2002. Investigation of impingement heat transfer coefficient at high temperatures. *Drying Technol.* **20**(1): 211–222.

Huber, A. M., Viskanta, R., 1994. Effect of jet-jet spacing on convective heat transfer to confined, impinging arrays of axisymmetric jets. *Int. J. Heat Mass Transfer* **37**: 2859–2869.

Martin, H., 1977. Heat and mass transfer between impinging gas jets and solid surface, in *Advances in heat transfer*, (eds J. R. Hartnett, T. F. Irvine), Academic Press, New York, USA, pp. 1–59.

McDaniel, C. S., Webb, B. W., 2000. Slot jet impingement heat transfer from circular cylinders. *Int. J. Heat Mass Transfer* **42**: 1975–1985.

Mujumdar, A. S. (ed.), 2007. *Handbook of industrial drying*, CRC Press, Boca Raton, USA.

Nada, S. A., 2006. Slot/slots air jet impinging cooling of a cylinder for different jets - cylinder configurations. *Heat Mass Transfer* **43**(2): 135–148.

Olsson, E. E. M., Ahrné, L. M., Trägardh, A. C., 2004. Heat transfer from a slot air jet impinging on a circular cylinder. *J. Food Eng.* **63**: 393–401.

Vader, D. T., Incropera, F. P., Viskanta, R., 1991. Local convective heat transfer from a heated surface to an impinging, planar jet of water. *Int. J. Heat Mass Transfer* **34**: 611–623.